Springer

Journal of
Mechanical
Science and
Technology

Journal of Mechanical Science and Technology 22 (2008) 1099~1110

www.springerlink.com/content/1738-494x

Trajectory optimization and the control of a re-entry vehicle in TAEM phase

Jo-Ha Baek[1], Dae-Woo Lee[1,*], Jong-Hun Kim[1], Kyeum-Rae Cho[1] and Jang-Sik Yang[2]

[1]*Dept of Aerospace Engineering, Pusan National University, Busan 609-735, Korea*
[2]*RIMT, Pusan National University, Busan 609-735, Korea*

(Manuscript Received May 10, 2007; Revised March 21, 2008; Accepted May 2, 2008)

Abstract

This paper investigates the optimal trajectory and the feedback linearization control of a re-entry vehicle during TAEM (terminal area energy management) phase. First, an optimization algorithm with dynamic pressure as the cost function is used to obtain the optimal trajectory in TAEM. This optimal trajectory is considered the reference for ensuring a stable flight path of the re-entry vehicle. The control inputs are the angle of attack and bank angle, which determine the total energy and safety of the re-entry vehicle. Second, feedback linearization is used to design a tracking law in the TAEM phase. This paper validates the optimal solution as the reference trajectory with HAC (heading alignment cylinder) and the tracking performance of the re-entry vehicle onto the reference trajectory by feedback linearization.

Keywords: Optimization; Re-entry vehicle; TAEM; HAC; Control; Feedback linearization

1. Introduction

In recent years, concerns about the re-entry space vehicle as a space transportation system have been increased according to service to the International Space Station (ISS). Because of this tendency, many countries have carried out a great deal of research on the re-entry space vehicle. Particularly, the problem of re-entry to earth has become very important. Re-entry consists of three phases: the entry phase, TAEM (terminal area energy management) phase, and A/L (approach and landing) phase. The TAEM phase, that is, the second phase of the re-entry stage, consists of an altitude region ranging from 3km to 27.5km in which the density, temperature, and sonic speed of the atmosphere vary with altitude. The re-entry vehicle is controlled by controlling the bank and angle of attack. Re-entry velocity in the TAEM phase ranges from the minimum, Mach 0.3, to the maximum, Mach 3. This velocity range includes subsonic, transonic, and supersonic velocities.

The flight objective in the TAEM phase must satisfy some of the requirements of the A/L phase threshold. In other words, it is energy dissipation during the TAEM phase, which means velocity adjustment for a stable landing of the re-entry space vehicle. In addition, the re-entry space vehicle should fly straight along the landing site. The limited conditions and criteria of valuation are needed to satisfy these requirements. According to the objective of the TAEM phase and the environment conditions, the vehicle in the TAEM phase is led to a peculiar trajectory profile to turn around HAC (heading alignment cylinder).

Recently, there has been extensive research on the entry phase and A/L phase [1, 2], but only few on the TAEM phase [3, 4], on which trajectory planning algorithms or control algorithms have focused. Research on the TAEM phase has been divided into several areas according to the method of approach. First, the reference trajectory is generated by two methods. One method relies on a pre-computed and stored database of a neighboring TAEM trajectory,

*Corresponding author. Tel.: +82 51 510 2329, Fax.: +82 51 513 3760
E-mail address: baenggi@pusan.ac.kr
DOI 10.1007/s12206-008-0501-y

and the other relies on a trajectory generation algorithm. Second, advanced guidance and control (AG & C) has been developed into various forms like fuzzy logic, neural network, adaptive critic neural network, etc. Finally, on-line trajectory-reshaping algorithms have been newly developed.

This paper presents a new optimum-path-to-go (OPTG) reference trajectory generation algorithm, different from other algorithms [3]. Generally, many studies have referred to the geometric trajectory generated by this algorithm as the reference trajectory. This algorithm divides the TAEM phase into acquisition, heading alignment cylinder (HAC) and pre-final according to flight characteristics. Furthermore, this paper obtains the reference trajectory by an optimal algorithm which includes the flight range and dynamic pressure as performance indices. This OPTG algorithm shows that the variation of flight range generates HAC and HAC's scale and shape. This is superior to the geometric trajectory generation method with respect to stability as well as optimal meaning. Moreover, we present the reference trajectory with two HACs which do not need more than one circular flying. For guidance, the feedback linearization law, which makes the re-entry vehicle track onto the reference trajectory, is used. This simple guidance law uses azimuth error to make the reentry vehicle track onto the reference trajectory. We verify the sufficient energy dissipation effect provided by the HACs generated by OPTG algorithm and the good tracking performance of the feedback linearization method.

2. Reference trajectory

2.1 Reference trajectory for the simplified re-entry vehicle model

In this chapter, we investigate the optimal trajectory problem for a simple reentry vehicle model before considering the maneuvering of the re-entry vehicle model with reality. This optimal trajectory becomes the reference which can be used to verify the effects of performance indices and constraints on the generation of the optimal trajectory. The following simple example will provide the idea of reference trajectory generation. A detailed algorithm will be presented in the next chapter 2.1.4.

The motion for a simplified reentry vehicle model can be described as shown Fig. 1. Fig. 1 shows only a

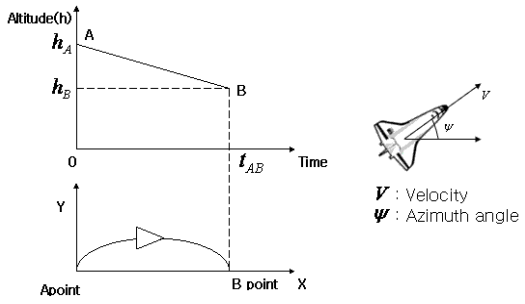

Fig. 1. Simplified re-entry vehicle model.

consideration of the horizon motion in the optimal trajectory. In this case, the following assumptions are made.

• The non-thrusting constant velocity (V) re-entry vehicle is assumed to be a point mass from the 2-D plane of the earth.

• Only gravity is considered as an external force.

From the above assumptions, we define the length L between points A and B in Cartesian coordinates as the flight trajectory. ψ is the azimuth angle between vectors x and V .

Eqs. (1)-(3) show the equations of motion for this model. The time variations of the geometric coordinates x and y are represented as velocity.

The time variation of the azimuth angle is represented as the control input u , and final time is fixed. For non-dimension, $\dot{x}$ and $\dot{y}$ are normalized by the velocity V , and the performance index of the optimal trajectory problem for this model is given by the square of u , as shown Eq. (4). Eq. (4) means that the optimized trajectory should have a slow variation of the azimuth angle during the TAEM phase; therefore, the burden on the control systems is reduced. The boundary conditions are given in Table.1. This optimization was carried out with SNOPT, which is one of the well-known numerical optimization methods that solves sparse NLP. SNOPT solves sparse nonlinear optimization problems. It is a general purpose system for contained optimization. It minimizes a linear or nonlinear function subject to the bounds on the variables and sparse linear or nonlinear constraints.

$$\dot{x} = V\cos\psi \tag{1}$$

$$\dot{y} = V\sin\psi \tag{2}$$

$$\dot{\psi} = u \tag{3}$$

$$J = \int_{t_0}^{t_f} u^2 \tag{4}$$

Table 1. Boundary conditions.

Initial condition	$X(t_0)=0$
	$Y(t_0)=0$
	$\Psi(t_0)=0$
Final condition	$X(t_f)=1$
	$Y(t_f)=0$
	$\Psi(t_f)=0$

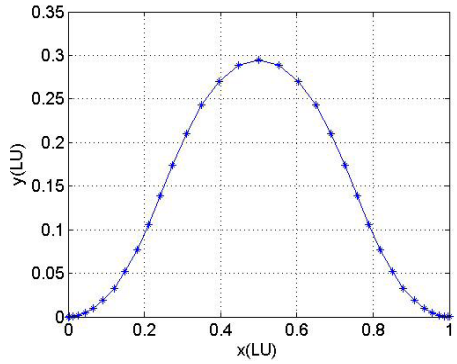

Fig. 2. Trajectory ($t_f = 1.2s$, $0 \le y \le 0.35$).

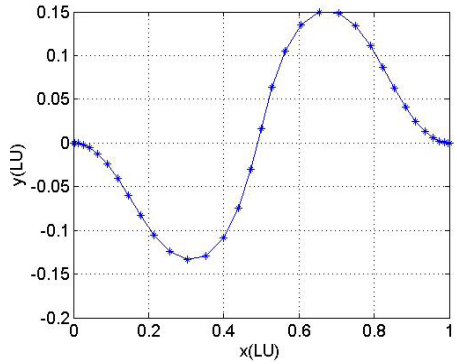

Fig. 3. Trajectory ($t_f = 1.2s$, $-0.15 \le y \le 0.15$).

3. Result of simulations

Figs. 2-5 show the fight trajectories for the simplified reentry vehicle model at final times of 1.2s and 4.0s. The key feature of the results is that the trajectory becomes longer as the final time increases. And the flight trajectories show various patterns according to the constraints of y. From these simple model results, we can expect trajectory maneuver for the reentry vehicle with reality.

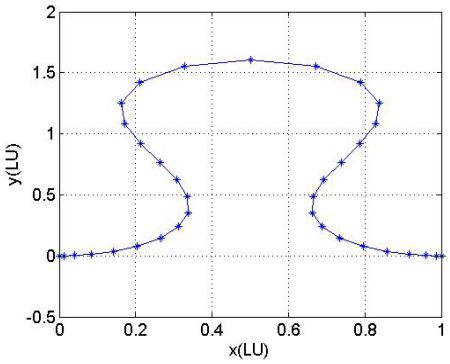

Fig. 4. Trajectory ($t_f = 4.0s$, $0 \le y \le 2$).

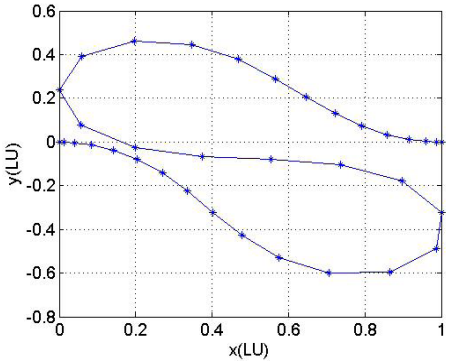

Fig. 5. Trajectory ($t_f = 4.0s$, $-0.6 \le y \le 0.6$).

2.2 The reference trajectory of the re-entry vehicle

The optimal trajectory of a re-entry vehicle with reality is similar to that of the simplified re-entry vehicle model in concept. However, in the case of a re-entry vehicle with reality, various parameters should be considered: temperature and density of atmosphere, and aero coefficients of the real model, etc. Especially, these parameters should be considered at the vertical maneuver because they vary according to the altitude. The general trajectory in the TAEM phase is shown in Fig. 6. Since the atmospheric density increases as the altitude of the trajectory, which starts from the TAEM interface, lowers, the vehicle can achieve the greatest energy dissipation when flying along the HAC near the A/L interface.

In this paper, the entry direction was assumed to be the same as that of the runway. As a result, two types of trajectories were expected, which is shown in Fig. 7. The 1st type corresponds to the movement of the vehicle gliding along only one HAC, while the 2nd type along two HACs. In the (a) type, a simple trajec-

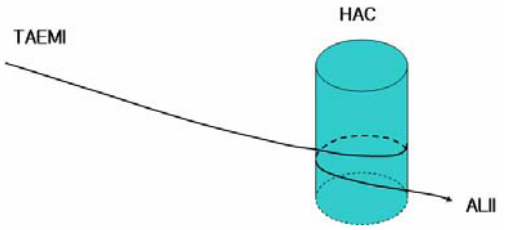

Fig. 6. General trajectory in TAEM.

Fig. 7. Two cases of trajectory.

tory is an advantage. However, the altitude control of the flight in this trajectory is difficult because the vehicle should fly in several circular maneuvers. Moreover, the sustained turns require that sufficient thrust be available to overcome the big drag in the turn. On the other hand, type (b) does not need more than one circular maneuver because the number of HAC is more than one. This type needs several HAC designs, which can be easily obtained by the optimal solution. And although this type needs an abrupt maneuver at the final HAC, altitude control is easier than that of type (a) because the final HAC is located on the runway. Therefore, we chose the type (b) as the HAC in this paper.

For the real model, we chose the Japanese re-entry vehicle Hope-X and obtained the optimal trajectory from DIDO, which is an optimal problem solver. This trajectory obtained by optimization is called the reference trajectory.

2.2.1 Re-entry space vehicle model

The re-entry space vehicle applied in this paper is HOPE-X, which was developed by the National Aerospace Laboratory and the National Aerospace Development Agency in Japan. The association of these agencies generated JAXA. HOPE-X has a mass (m) of 8150kg and reference area (A) of 65m^2. Aero coefficients of HOPE-X were taken from reference [6] as shown in Figs. 8 and 9. Because of the lack of data below Mach number 0.4, aero coefficients for this velocity region were presumed to be constant. Unfortunately, the velocity at final condition was about Mach number 0.3, and therefore, low reliability

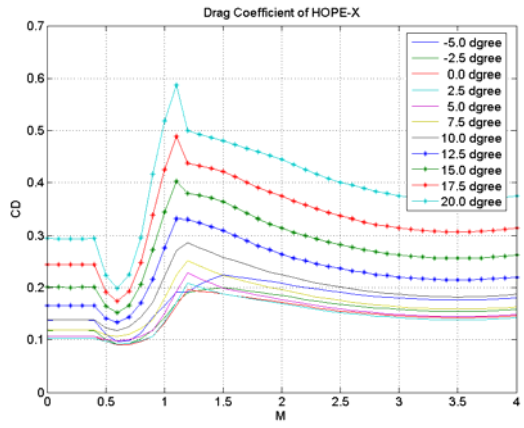

Fig. 8. Drag coefficients of HOPE-X.

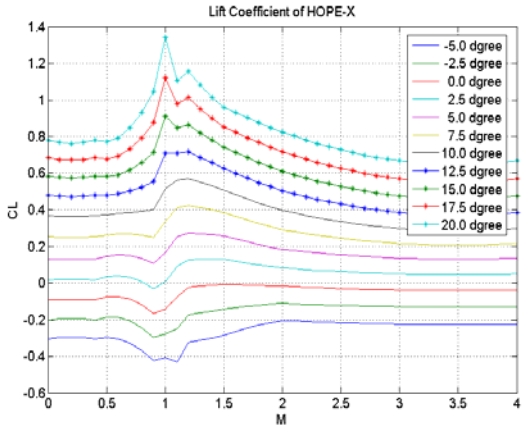

Fig. 9. Lift coefficients of HOPE-X.

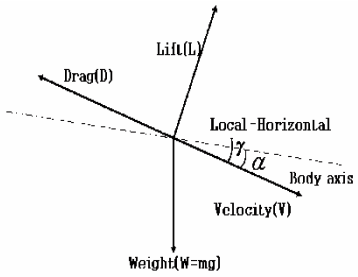

Fig. 10. Free-body diagram of reentry vehicle.

was expected for the final region.

2.2.2 Equations of motion

The earth was considered to be a 2-dimensional surface, and the flight of a point mass re-entry vehicle was characterized as pure gliding without thrust. Fig. 10 shows the vectors acting on the center of the air-

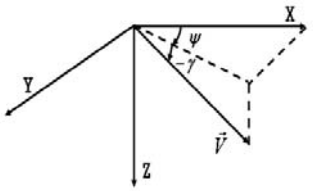

Fig. 11. Coordinates about azimuth and flight path angle.

frame. These vectors represent velocity (V), lift (L), drag (D), and weight (W). The flight path angle is γ , and the angle of attack is α . Fig. 11 describes the direction of the velocity vector in terms of the flight path angle (γ) and azimuth angle (ψ). In this figure, γ has a negative value.

With consideration of this serialized coordinate transformation and gliding condition, its gliding dynamics is defined by

$$\dot{V} = -\frac{D}{m} - g\sin\gamma \tag{5}$$

$$\dot{\gamma} = \frac{L\cos\sigma}{mV} - \frac{g}{V}\cos\gamma \tag{6}$$

$$\dot{\psi} = \frac{L\sin\sigma}{mV\cos\gamma} \tag{7}$$

$$\dot{h} = V\sin\gamma \tag{8}$$

$$\dot{x} = V\cos\gamma\cos\psi \tag{9}$$

$$\dot{y} = V\cos\gamma\sin\psi \tag{10}$$

$$D = \frac{\rho A C_D V^2}{2},\quad L = \frac{\rho A C_L V^2}{2} \tag{11}$$

where m is the mass, g is the gravitational acceleration, σ is the bank angle, h is the altitude, and x and y are the 2-D positions.

Lift and drag coefficient are defined by the Mach number and angle of attack, and the Mach number is affected by the density and temperature:

$$C_L = C_L(\alpha, M),\quad C_D = C_D(\alpha, M) \tag{12}$$

The dynamic pressure (q) is defined as $\rho V^2/2$. The atmospheric density ρ is exponentially varying.

$$\rho = \rho_0 \exp\left(-\frac{R - R_0}{h_s}\right) \tag{13}$$

where ρ_0 is the density at sea level, $h = R - R_0$ is the altitude, and h_s is the density scale-height. From the Eq. (13), we can derive the radial distance from the earth center to the vehicle.

$$R = R_0 - h_s \log\left(\frac{\rho}{\rho_0}\right) \tag{14}$$

Substituting ρ of Eq. (11) into Eq. (14),

$$h = R - R_0 = -h_s \log\left(\frac{2Dm}{V^2 A_{ref} C_D \rho_0}\right) \tag{15}$$

2.2.3 Optimization

The optimization problem

If the system has dynamic constraints, it is represented by

$$\dot{\boldsymbol{x}} = f(\boldsymbol{x}, \boldsymbol{u}, \tau) \tag{16}$$

where $\boldsymbol{f}$ is the vector of functions that describe the dynamics of the system, $\boldsymbol{x}$ is the vector of states that describe the system at any time τ , and $\boldsymbol{u}$ is the vector of the control variables. The system is assumed to be subjected to constraints that include the path constraint of the form

$$\boldsymbol{h}_l \le \boldsymbol{h}(\boldsymbol{x}, \boldsymbol{u}, \tau) \le \boldsymbol{h}_u \tag{17}$$

where h is the vector of functions that describe the path constraints, h_l is the vector of the lower path bounds and h_u is the vector of the upper path bounds. The boundary conditions are given as

$$\boldsymbol{e}_l \le \boldsymbol{e}(\boldsymbol{x}(\tau_0), \boldsymbol{x}(\tau_f), \tau_0, \tau_f) \le \boldsymbol{e}_u \tag{18}$$

where $\boldsymbol{e}(\boldsymbol{x}(\tau_0), \tau_0)$ is the vector of initial boundary conditions at τ_0 , $\boldsymbol{e}(\boldsymbol{x}(\tau_f), \tau_f)$ is the vector of final boundary conditions at τ_f , $\boldsymbol{e}_l$ is the vector of lower bounds, and $\boldsymbol{e}_u$ is the vector of upper bounds. The system has bounds on the control and state variables, as well, represented by

$$\begin{aligned} &\boldsymbol{x}_l \le \boldsymbol{x}(\tau) \le \boldsymbol{x}_u \\ &\boldsymbol{u}_l(\boldsymbol{x}) \le \boldsymbol{u}(\tau) \le \boldsymbol{u}_u(\boldsymbol{x}) \end{aligned} \tag{19}$$

An optimal control problem seeks to determine the solution that will minimize the given performance index of the preceding dynamical system under its bounds and constraints. The general optimal control problem is posed in the following manner.

$$\begin{aligned} &\min J(\boldsymbol{x}(\tau), \boldsymbol{u}(\tau), \tau_0, \tau_f) = \\ &E(\boldsymbol{x}(\tau_0), \boldsymbol{x}(\tau_f), \tau_0, \tau_f) + \int_{\tau_0}^{\tau_f} F(\boldsymbol{x}(\tau), \boldsymbol{u}(\tau), \tau) d\tau \end{aligned} \tag{20}$$

where E is the scalar cost function evaluated at the boundaries and F is the scalar cost function evaluated over the entire interval. The formulation of the system forms the basis of the optimal control problem.

Solution method

Once the problem has been properly formulated, two types of general methods, namely, the direct and the indirect methods, can be used to solve the optimal control problem. Indirect methods generate fast solution times and good accuracy but are more difficult to formulate and are very sensitive to the initial guess. Formulation of the indirect method can be difficult in situations where the dynamics functions are not pure functions. Direct methods reduce the optimal control problem to a single large nonlinear programming (NLP) problem. The direct methods are advantageous because their formulations are much easier and are relatively insensitive to the initial guess.

This paper uses the DIDO numerical dynamic optimization software developed by I. M. Ross and F. Fahroo. DIDO employs a direct Legendre pseudospectral technique that uses the NLP solver SNOPT and covector mapping theorem (CMT), which links the solutions generated by the indirect methods and the direct methods. Because the DIDO solution is based on the controls for a discretized set of points determined by the Legendre polynomials used in the solution, the DIDO solution may not have the desired accuracy at the final point. Feedback may be able to overcome this inaccuracy if the solution is updated at a reasonable rate.

SNOPT is an NLP solver included in DIDO to solve optimal problems.

Optimal trajectory in TAEM

In this paper, the boundary conditions for the TAEM maneuver were defined completely. The initial conditions were collected to form a set of navigation parameters, and the final conditions were the target parameters for the A/L (Approach/ Landing) phase. The bank angle was also set along the direction of the runway at the initial stage of TAEM.

The objectives of the optimal trajectory in the TAEM phase are a guarantee of the re-entry vehicle's stability and decrease of sufficient energy to begin the A/L phase. Moreover, the reentry vehicle flies straight along the runway at the TAEM final region.

In this paper, the reference trajectory is represented as a stability and energy reduction. The stability is guaranteed by the minimization of the difference between the pre-set target dynamic pressure and the dynamic pressure at the actual altitude, and energy can be reduced by minimizing the difference between the final flight range and pre-desired final flight range.

Eq. (21) shows the performance index for the dynamic pressure and flight range.

$$MinJ = (S - S_{target})^2 + \int_{t_0}^{t_f} \left(\frac{q - q_{target}}{q_{target}} \right)^2 dt \qquad (21)$$

where S is the flight range, S_{target} is 90km as a target flight range, and q_{target} is the target dynamic pressure.

Eq. (22) shows the bounds on the control vectors. The control vectors are metrics of the bank angle and angle of attack

$$\begin{bmatrix} -90^0 \\ -90^0 \end{bmatrix} \le \boldsymbol{u}(\tau) \le \begin{bmatrix} 90^0 \\ 90^0 \end{bmatrix} \qquad (22)$$

where $\boldsymbol{u}(\tau) = [\boldsymbol{\sigma}(\tau); \boldsymbol{\alpha}(\tau)]$. The initial and final boundary conditions mean the values at Re-Entry & TAEM Interface and TAEM & A/L Interface, respectively. These conditions are

$$\boldsymbol{e}(\boldsymbol{x}(\tau_0), \tau_0) = \boldsymbol{x}_i = \begin{bmatrix} \boldsymbol{x_i} \\ \boldsymbol{y_i} \\ \boldsymbol{z_i} \\ \boldsymbol{V_i} \\ \boldsymbol{\gamma_i} \\ \boldsymbol{\psi}_i \end{bmatrix} = \begin{bmatrix} -6\times10^3 m \\ 0m \\ 27500m \\ 760m/s \\ -6.74^0 \\ 0^0 \end{bmatrix} \qquad (23)$$

$$\boldsymbol{e}(\boldsymbol{x}(\tau_f), \tau_f) = \boldsymbol{x}_f = \begin{bmatrix} \boldsymbol{x}_f \\ \boldsymbol{y}_f \\ \boldsymbol{z}_f \\ \boldsymbol{V}_f \\ \boldsymbol{\gamma}_f \\ \boldsymbol{\psi}_f \end{bmatrix} = \begin{bmatrix} 0m \\ 0m \\ 3\times10^3 m \\ 162m/s \\ -15.9^0 \\ 0^0 \end{bmatrix} \qquad (24)$$

and constraints on the state variables:

$$\begin{bmatrix} -95\times10^3 m \\ 0m \\ 3\times10^3 m \\ 1\times10^2 m/s \\ -90^0 \\ -360^0 \end{bmatrix} \le x \le \begin{bmatrix} 1\times10^4 m \\ 3\times10^4 m \\ 3\times10^4 m \\ 800m/s \\ 90^0 \\ 360^0 \end{bmatrix} \qquad (25)$$

Constraints on the state variables can set a more broad region, but this method needs more calculation time. So, we can reduce or narrow the gap between

the lower and upper bounds within a physically reasonable range.

2.2.4 Result of optimization

The initial condition of downrange (x) and cross-range (y) is (-60km, 0), and the final condition is (0, 0), which is the threshold point of ALI (Approach/Landing Interface). The target dynamic pressure in a performance index is chosen as regards physical condition. In this paper, this value is 7,500Pa. Figs. 12 and 13 show the optimal flight trajectory in 2-D and 3-D, respectively. These figures show that the vehicle lowers its altitude to control the attitude because attitude can be controlled at low altitude, where dynamic pressure is high. We can verify that two HAC are generated in this paper, as previously expected. Fig. 14 shows the earth relative velocity time history. The tendency of a sudden increase in the final region is because the flight path angle increases rapidly in the minus direction as shown in Fig. 15. Rapid variation of the flight path angle is due to the 2nd HAC. In other words, an abrupt maneuver is needed to flight onto a small radius 2nd HAC. Fig. 16 shows an azimuth angle, and Fig. 17 shows if a flight range satisfies the reference flight range of 90km or not. Figs. 18 and 19 represent the aerodynamic coefficient time histories used in this optimization. The atmospheric density and dynamic pressure are represented in Figs. 20 and 21, respectively. There is a difference between the optimal dynamic pressure and the reference value because it is impossible to sustain a constant dynamic pressure due to the physical condition of initial and final points according to the altitude. Fig. 22 shows the Hamiltonian time history. For this problem, since the Hamiltonian is not an explicit function of time and the terminal time is free, the Hamiltonian along an optimal trajectory must be zero. From Fig. 22, the Hamiltonian oscillates about zero and its magnitude remains very small throughout the trajectory. Figs. 23 and 24 show the angle of attack and bank angle along an optimal trajectory, respectively. The results obtained from Figs. 22-24 give strong evidence that the trajectory obtained from this TAEM formula is close to the optimal trajectory.

Fig. 25 shows the 2-D reference trajectories along the HACs according to the flight ranges of 70km, 80km, and 90km. From Fig. 25, we can verify that the radius of the 1st HAC changes and that the ratio of the energy dissipation increases in the 1st HAC according to the flight ranges. This result means that these trajectories reduce the control load as the variation of the dynamic pressure is reduced. We can verify that the small radius of the 2nd HAC does not vary according to the range, but this one requires an abrupt turn maneuver.

After the flight along the 1st HAC, the atmospheric density becomes relatively higher, so high drag is generated, which enables the vehicle to dissipate more energy. That is, although the radius of the 2st HAC is small, energy dissipation is sufficient. The

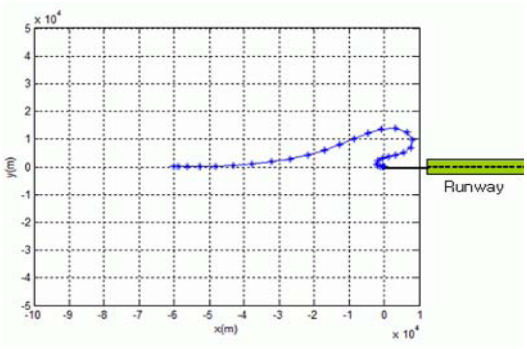

Fig. 12. 2-D optimal trajectory.

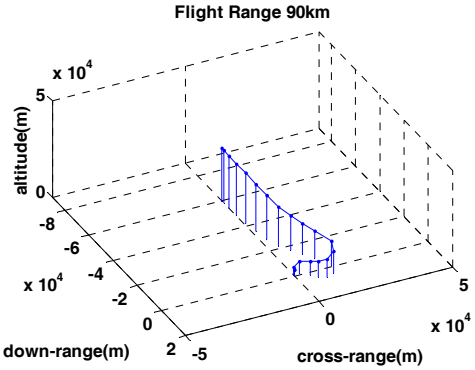

Fig. 13. 3-D optimal trajectory.

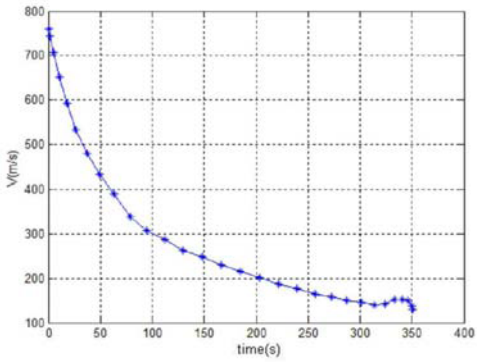

Fig. 14. Velocity.

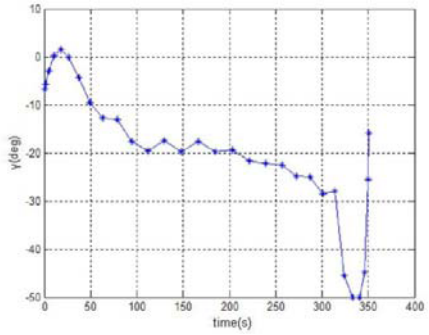

Fig. 15. Flight path angle.

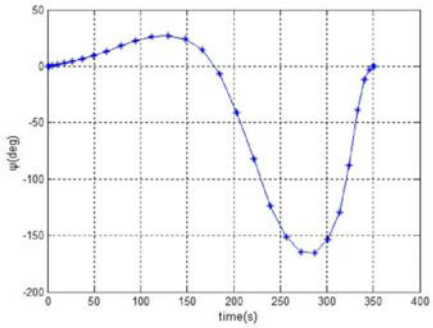

Fig. 16. Azimuth angle.

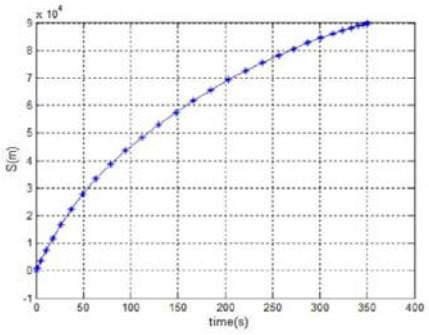

Fig. 17. Range.

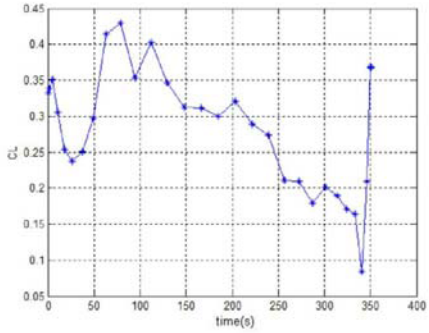

Fig. 18. Coefficients of lift.

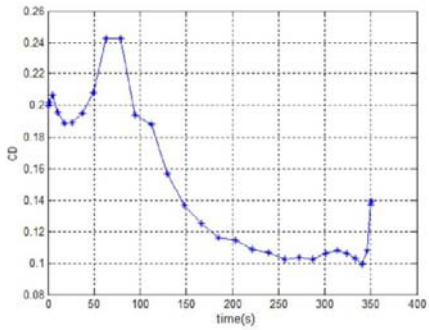

Fig. 19. Coefficients of drag.

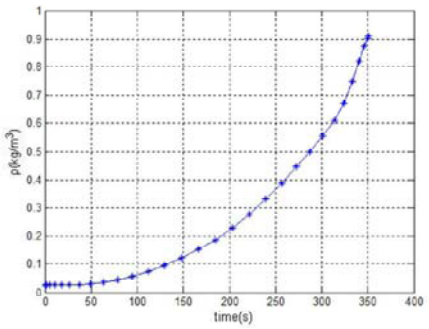

Fig. 20. Atmosphic density.

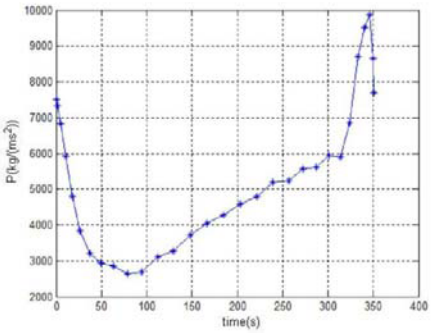

Fig. 21. Dynamic pressure.

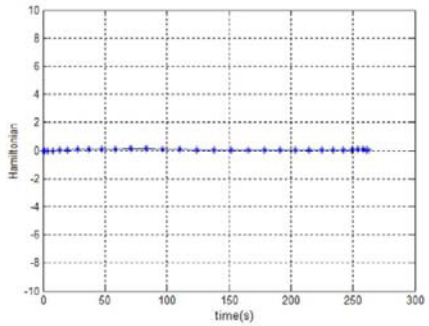

Fig. 22. Hamiltonian value.

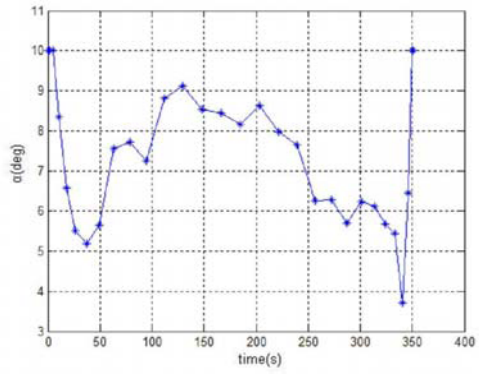

Fig. 23. Angle of attack.

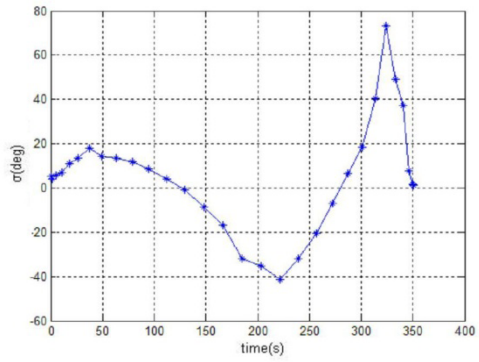

Fig. 24. Bank angle.

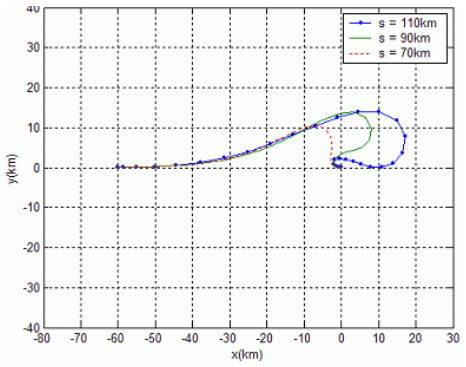

Fig. 25. 2-D Reference trajectories.

magnitude of the bank angle increases dramatically during the 2nd turn and it reduces the lift force so that the flight path angle reaches a maximum of 50 degrees in the negative direction. To satisfy the final states in the TAEM phase, the flight path angle needs to be finally increased to the requirement of the final condition. As a result, the flight path angle changes rapidly around ALI.

3. Tracking onto the reference trajectory

The aforementioned optimal trajectory is the reference trajectory. To track onto this, adequate control law is necessary. This paper presents a feedback linearization using azimuth errors to guide the reentry vehicle onto the reference trajectory.

3.1 Feedback linearization

Feedback linearization [7] is an approach to nonlinear control design. The central idea of the approach is to algebraically transform nonlinear system dynamics into a fully/partly linear one, so that linear control technique can be applied. In other words, this method generates the same response as that of a linear system, which excludes nonlinear characteristics. Feedback linearization has been used successfully to address some practical control problems in fields including industrial robots, biomedical devices, helicopters as well as high performance space vehicles.

In this paper, among the states, the error of the azimuth angle [8] is only used as the feedback state. Because the time derivative of the azimuth angle is related to the bank angle as shown in Eq. (7), it is useful to control the azimuth angle in the 2-D plane. Also, the other states can be expressed as the relationship about the azimuth angle.

The tracking errors for the control law are Eq. (26)

$$\begin{aligned} \Delta\psi &= \psi - \psi_{ref} \\ \Delta\dot{\psi} &= \dot{\psi} - \dot{\psi}_{ref} \end{aligned} \tag{26}$$

Assuming that the response of the tracking error $\Delta\psi$ in Eq. (26) is that of the no-input linear first system with natural frequency ω_n and damping coefficient, ξ,

$$2\xi w_n \Delta\dot{\psi} + w^2{}_n \Delta\psi = 0 \tag{27}$$

Substituting $\Delta\psi$, and $\Delta\dot{\psi}$ as given by Eq. (26), the following is derived

$$2\xi w_n \left(\dot{\psi} - \dot{\psi}_{\mathrm{Re}f}\right) + w_n{}^2 \left(\psi - \psi_{\mathrm{Re}f}\right) = 0 \tag{28}$$

Substituting Eq. (7) into Eq. (28), we have

$$\sin\sigma = \frac{mV\cos\gamma}{2w_n\xi L}\left(2\xi w_n \dot{\psi}_{\mathrm{Re}f} - w_n{}^2\left(\psi - \psi_{\mathrm{Re}f}\right)\right) \tag{29}$$

$$\sigma = \sin^{-1}\left(\frac{mV\cos\gamma}{2w_n\xi L}\left(2\xi w_n \dot{\psi}_{\mathrm{Re}f} - w_n{}^2\left(\psi - \psi_{\mathrm{Re}f}\right)\right)\right) \tag{30}$$

These values can be used as indices to determine

the control gain.

3.2 Result of tracking

In this paper, because angle of attack is determined along the reference angle of attack, the bank angle is considered only as the control input. Fig. 26 shows a good tracking performance of the azimuth angle. The maximum error is 0.8 degree. From Fig. 27, it is seen that the bank angle history has some tracking error at the final region. Fig. 28 shows the flight path angle. Though there is some error at the final region like Fig. 27, tracking performance is good overall. Fig. 29 presents the earth's relative velocity, whose maximum error is 3m/s at 325 second, but after this time, the maximum error is 5.5m/s. Figs. 30-32 show the altitude, down-range, and cross-range, respectively. Fig. 33 shows flight trajectory in the x-y coordinate plane. Fig. 34 presents the errors of the down-range, cross-range, and altitude. The maximum error of the down-range is about 170m around 230 seconds, whose maximum error of the cross-range is about-175m around the final time. The maximum error of the altitude is about 473m around the final time.

The tracking errors increase around 325 seconds because in this region, the angle of attack and aerodynamic coefficients, which are obtained by optimization, change rapidly. In other words, these phenomena are caused by uncertainties of aerodynamic coefficients. Though the final errors are relatively large, these can be compensated by the activity in the A/L phase.

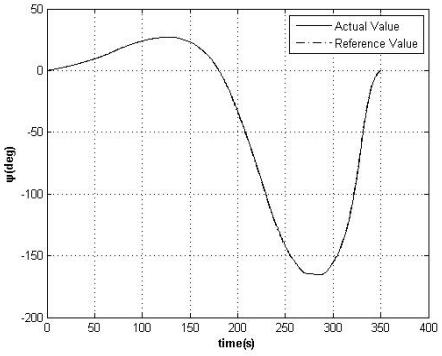

Fig. 26. Azimuth angle.

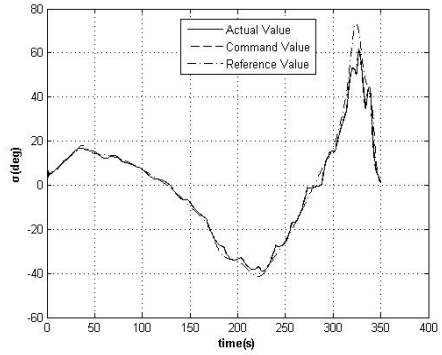

Fig. 27. Bank angle.

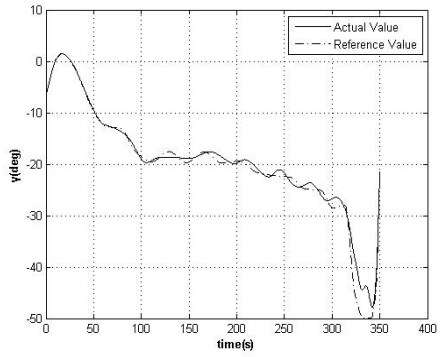

Fig. 28. Flight path angle.

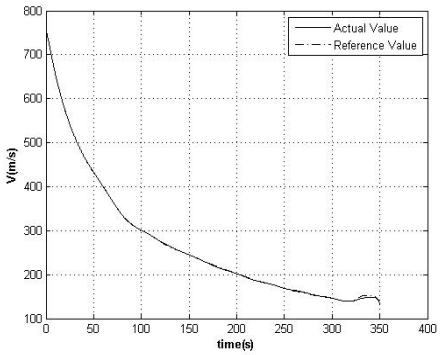

Fig. 29. Velocity.

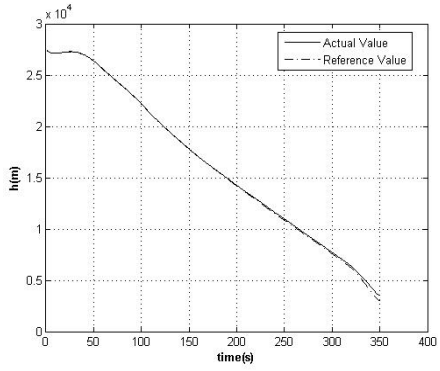

Fig. 30. Altitude.

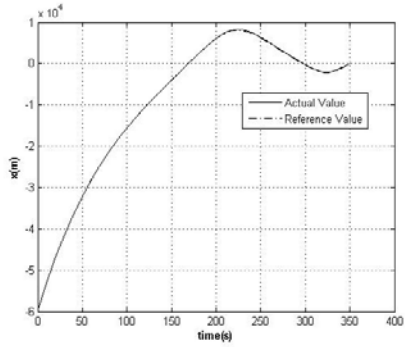

Fig. 31. Downrange (x).

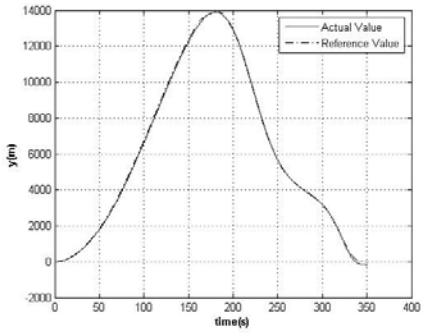

Fig. 32. Cross-range (y).

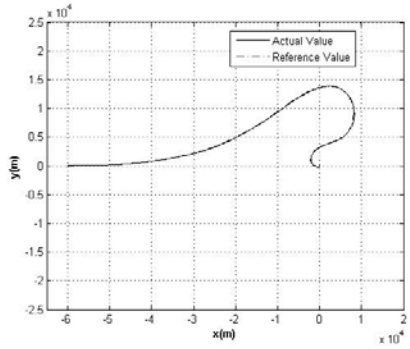

Fig. 33. Geometric flight trajectory.

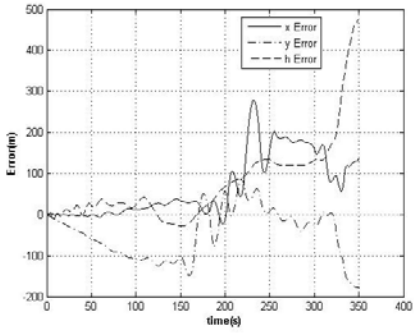

Fig. 34. Error of x, y, z.

4. Conclusions

Because the variation of density and temperature in the TAEM phase is sufficiently large and all of the sonic regions, that is, supersonic, transonic, and subsonic regions, had to be considered, there has been less research about TAEM than about the other three phases of re-entry. However, recently, interest in the guidance/control of the reentry vehicle at the TAEM phase has increased because of the importance of TAEM research and advancements in computation.

This paper presented the reference trajectory via OPTG algorithm with minimum variation of dynamic pressure, the flight range as a performance index, and feedback linearization as the guidance scheme for the TAEM phase of a gliding re-entry vehicle. Variation of flight range determined the scale of the 1st HAC, which determined energy dissipation. Although 2nd HAC had small radius, abrupt turns could incur sufficient energy dissipation. These results expand on guidance performance in TAEM phase. The obtained reference trajectory was demonstrated as the optimal one by the Hamiltonian result. Although there were some errors around the final time, this system showed good tracking performance because these errors are enough to reduce in the A/L phase.

Acknowledgment

"This paper was supported by the Korea Research Foundation Grant funded by the Korean Government (MOEHRD)" (KRF-2005-003-D00059)

References

[1] A. Saraf, J. A. Leavitt, D. T. Chen and K. D. Mease, Design and evaluation of an acceleration guidance algorithm for entry, Journal of Spacecraft and Rockets. 41 (6) (2004) 986-996.

[2] B. N. Pamadi and G. J. Brauckman, Aerodynamic characteristics and development of the aerodynamic database of the X-34 reusable launch vehicle, International Symposium on Atmospheric Reentry Vehicles and Systems, Arcachon, France (1999).

[3] K. R. Horneman and C. A. Kluever, Terminal area energy management trajectory planning for an unpowered reusable launch vehicle, AIAA Atmospheric Flight Mechanics Conference and Exhibit (2004).

[4] T. E. Moore, Space shuttle entry terminal area energy management, NASA TM-104744 (1991).

[5] G. H. Barton and Lt. A. C. Grubler USN and Lt. T. R. Dyckman USN, New methodologies for onboard generation of TAEM trajectories for autonomous RLVs, 2002 Core Technologies for Space Systems Conference (2002).

[6] K. H. Kim and C. Park, Conceptual design of a rocket-powered plane and its use for space tourism, KSAS International Journal, 6 (2) (2005) 46-55.

[7] J. J. E. Slotine and W. Li., Applied Nonlinear Control, Prientice Hall, USA (1991).

[8] J. W. Kraemer, Shuttle Orbiter Guidance System Fot the Terminal Flight Phase, Proceedings of the IFAC 6th World Congress (1975).